THE DYNAMIC MODELING OF AN ELECTRIC ARC FURNACE

Sam A. Matson, W. Fred Ramirez*, The University of Colorado at Boulder, and Paykan Safe, Goodfellow Consultants Texas, Inc.
*(303) 492-8660

1 INTRODUCTION

There have been continual improvements in the efficiency and control of the electric arc furnace (EAF) operation[1]. Sources for improvements usually come from knowledge of a particular aspect of steel-making such as physical chemistry, heat transfer, reactor design, or thermodynamics. Application of new ideas in these areas has lead to gradual improvements in the EAF steel-making process.

A fundamental model of the EAF steel-making process is useful in evaluating several process modifications simultaneously and discovering their effect on off-gas and bath compositions. An appropriately formulated model is also ideal for use in determining optimal operating strategies that achieve an extremum of a performance objective.

The literature on modeling of an EAF is sparse. This is probably due to both the proprietary nature of the results and the complexity of the problem. Early papers discuss simple models involving only a few compounds and reactions and only applied to flat bath conditions[2,3,4]. Recent industrial desire for further furnace optimization has created the the need for a complete model.

2 MODEL DEVELOPMENT

In developing an accurate model different events, causes, and effects in the furnace must be taken into account. Most importantly, the furnace model must include the scrap melting rate, the furnace chemistry, and the furnace material balance as well as the furnace operations like oxygen lancing, carbon injection, and burner operation.

For modeling purposes, the furnace interior is divided into two well-mixed control volumes. The gas control volume (GCV) is made up only of the free-board gases while the bath control volume (BCV) contains the bath, slag, and some gas. This arrangement is shown in Figure 1. Chemical reactions and furnace operations are assumed to take place within a control volume.

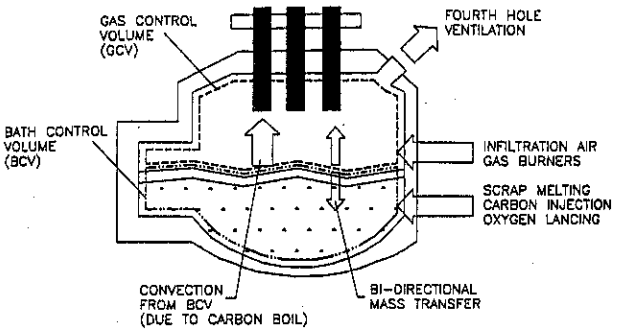

Figure 1: Furnace Model Control Volumes

2.1 Melting

The melting rate of scrap is an important part of the model because the amount of liquid iron present in the furnace determines the extent of some of the chemical reactions. A melting rate of zero indicates that the scrap has been melted completely and the bath temperature may be rising if energy is still being added to the furnace. Most of the energy that melts the scrap is the electrical energy that is supplied through the electrodes. The burners and exothermic chemical reactions provide additional energy to melt the charge.

The wide variation in the scrap shape and size requires making a simplifying assumption in order to make the melting model less complex. Our model assumes that the scrap is made up of n identical spheres of radius R. This simplification allows for heat transfer to one sphere to be modeled and scaled up for n spheres.

Since the scrap does not start out at the melting temperature, energy put into the scrap can go either to the sensible heat, raising the temperature or to latent heat, producing liquid. When the temperature of a differential volume of solid reaches the melting temperature, any additional energy transfered to the volume melts all or part of the volume.

The transfer of sensible heat to a sphere is described by equation 1, a partial differential equation (PDE) which equates the rate of energy accumulation to the rate of conduction. Equation 1 describes only temperature change, so an additional equation is needed to describe melting.

$$\frac{\partial T}{\partial t} = \frac{\alpha}{r^2}\frac{\partial}{\partial r}\left(r^2\frac{\partial T}{\partial r}\right) \qquad (1)$$

T	temperature
t	time
r	radial distance
α	thermal diffusivity $k/(\rho C_p)$
ρ	density
C_p	heat capacity
k	thermal conductivity

A modified finite difference method using equation 1 has been used for the EAF melting model. Derivatives in space have been converted to their finite difference forms, and the derivative in time remains for solution with an ordinary differential equation (ODE) integrator. Melting will reduce the sphere's radius, so the radial variable has been scaled:

$$r^* = \frac{r}{R(t)} \tag{2}$$

r^*	dimensionless radius
r	radius
$R(t)$	outer sphere radius

This substitution forces the r^* value to be between zero and unity inside of the sphere. The modified finite difference form of equation 1 is:

$$\frac{dT_i}{dt} = \frac{\alpha}{R^2}\left(\frac{2(T_{i+1}-T_i)}{r_i^*\Delta r^*} + \frac{T_{i-1}-2T_i+T_{i-1}}{\Delta r^{*\,2}}\right) \tag{3}$$

T_i	temperature at point r_i^*
α	thermal diffusivity
r_i^*	dimensionless length in radial direction
Δr^*	dimensionless distance between space points
$i = 1$	center of sphere

The boundary conditions imposed on the system are given in Table I. A symmetry condition is used at the sphere's center, while a heat flux condition is used at

Table I: Boundary Conditions

Location	Condition	Description
$r^* = 0$	$\frac{\partial T}{\partial r^*} = 0$	symmetry
$r^* = 1$	$flux = -k\frac{\partial T}{\partial r^*}$	surface flux

the surface. The heat flux to the surface is the total energy (electrical and chemical) available divided over the surface area of all n spheres.

A singularity in equation 3 exists at the center of the sphere, so evaluation must be performed carefully. Thibault presented the application of L'Hôpital's Rule for the evaluation at the origin[5]:

$$\lim_{r\to 0} \frac{\alpha}{r^{*\,2}}\frac{\partial}{\partial r^*}\left(r^{*\,2}\frac{\partial T}{\partial r^*}\right) = 3\alpha\frac{\partial^2 T}{\partial r^{*\,2}} \tag{4}$$

The first ODE is obtained by translating this continuous equation into its finite difference expression, and using symmetry to define $T_0 = T_2$:

$$\frac{dT_1}{dt} = 6\alpha\frac{T_2 - T_1}{\Delta r^{*\,2}} \tag{5}$$

This finite difference scheme handles heat transfer, excluding melting, accurately. In order to simulate both the melting and sensible heat transfer, the finite difference ODEs must be augmented with a melting algorithm. The melting portion monitors the temperature profile of the sphere and when an entire shell of the sphere is above the melting temperature, it triggers a melting routine for one time step which reduces the radius of the iron sphere. During a melting time step no sensible heat transfer takes place, making the accuracy of this method poor unless small time steps are used. The use of a small mesh in the space dimension is also necessary to maintain accuracy or else an entire shell cannot be melted in one time step. The change in radius of the sphere during a melting time step is expressed in equation 6.

$$\frac{dR}{dt} = \frac{Energy\ Rate}{4\pi \cdot \Delta H_{melt} \cdot \rho_{solid} \cdot R^2} \tag{6}$$

R	outer sphere radius
t	time
$Energy\ Rate$	chemical and electrical energy
ΔH_{melt}	heat of fusion of steel
ρ_{solid}	density of solid scrap

Figure 2 shows a plot of liquid volume verses time for a run with a 100 ton charge, constant electrical input of 70 MW (20.16 kW-hr/s), and an initial sphere radius of 10 cm. The figure shows a time delay followed by a linear rise in liquid volume for most of the melting regime. Figure 3 shows the sphere radius verses time for the same simulation. The simulation predicts an exponential drop in radius after the time delay. The time delay occurs because the scrap must be brought to its melting temperature before melting begins and the radius decreases.

The simulation predicts complete melt-out at 24.0 minutes for a time step size of 5 seconds and 21 finite difference points in space. A macroscopic energy balance shows that a total of 30,300 kW-hr is needed to melt this charge, which means that it should take 30,300 (kW-hr)/20.6 (kW-hr/s) = 24.5 minutes to melt. An industrial furnace typically uses 20 to 22 minutes to melt the charge. The shorter time in the industrial furnace is due to chemical energy contributions that are not modeled in the stand-alone melting model.

The sphere radius does not have any effect on the predicted time for complete melt-out, but does change the

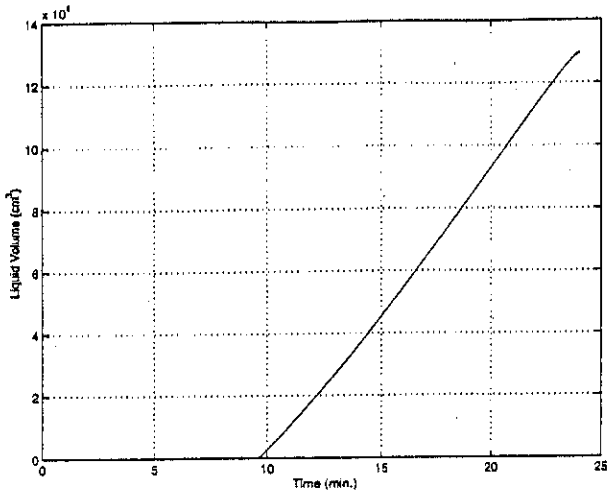

Figure 2: Liquid Volume vs. Time

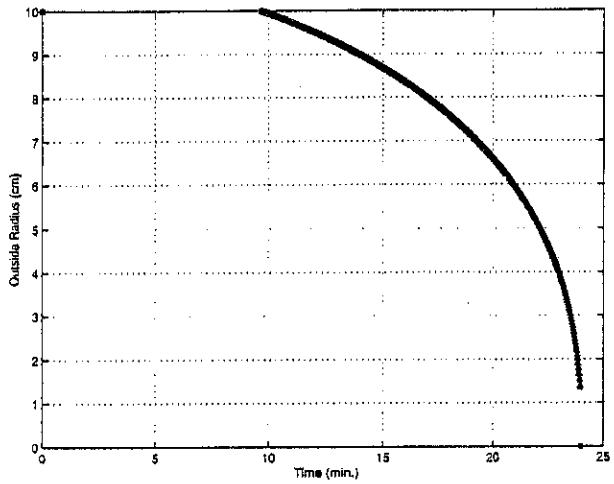

Figure 3: Sphere Radius vs. Time

time delay before melting starts. Figure 4 shows the results of several melting simulations with varying sphere radius. The larger the radius, the smaller the time delay before liquid is produced. If these findings are taken to the extreme, an infinitely small sphere would have a time delay approaching the total melting time, and an infinitely large sphere would begin to melt immediately.

The linear change in bath volume over most of the melting period is simple, and can be verified in the field. If field measurements show a non-linear profile, the model can be modified by using a distribution of sphere sizes to represent the diverse scrap shapes. If field measurements show a strong correlation between the furnace electrical input profile and the liquid production rate, a non-constant electrical schedule will have to be incorporated into the model.

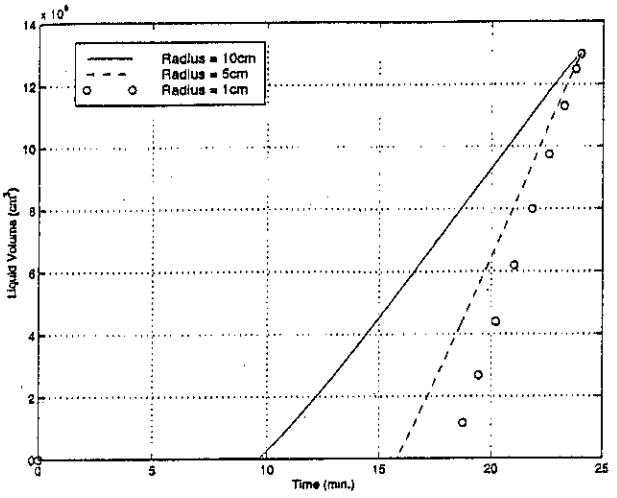

Figure 4: Effect of Radius on the Time Delay

2.2 Furnace Chemistry

Because there is a large number of compounds present in the three phases of the furnace, a simplification is necessary in order to create a model of lower complexity. The rationale used to choose the compounds is to include the compounds of interest as well as their pre-cursors. For example, we are interested in the off-gas composition, so CO, CO_2, H_2, O_2, N_2, and H_2O must be included in the model. In addition, species that may react to form these gases must also be included. These include dissolved oxygen in the bath ($\underline{O}$), dissolved hydrogen in the bath ($\underline{H}$), and carbon dissolved in the bath $\underline{C}$ [6,7,8]. The amounts of iron and iron oxide present are also important, so they are included as well. The compounds included in the model are shown in Figure 5.

After selecting the compounds to include in the model, the chemical reactions that consume or produce each compound must be selected. A set of six independent chemical reactions, shown in Table II, represent the reactions that take place in the bath control volume and two combustion reactions take place in the gas control volume of the furnace. At operating temperatures of 2800°F (1810K) the steel-making reactions are not limited by kinetics[8,9]. For this reason the set of eight chemical reactions are assumed to be at equilibrium at all times during the simulation. The furnace model is limited by mass transfer effects across the control volumes instead of kinetics. The modeling of the mass transfer limitations are developed in this paper.

The assumption of chemical equilibrium yields a set of eight algebraic constraints on the system that correspond to the eight chemical reactions. Since the amounts of 17 compounds must be found, nine more constraints must be set in order to obtain a unique solution for the amounts of each compound. Seven of these constraints come from the necessity for the conservation of atomic mass in the system. These seven relations make sure that the atomic

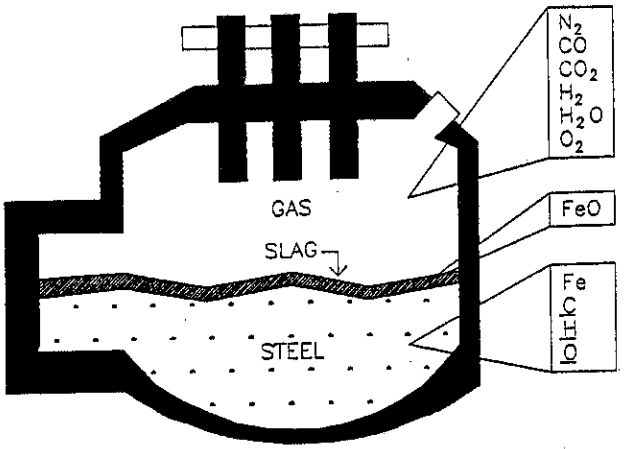

Figure 5: Furnace Compounds

Table II: Furnace Chemical Reactions

No.	Reaction
Bath Control Volume Reactions	
1B	$\frac{1}{2}O_2(g) + Fe(l) \rightleftharpoons (FeO)$
2B	$\frac{1}{2}O_2(g) \rightleftharpoons \underline{O}$
3B*	$\underline{C} + \underline{O} \rightleftharpoons CO(g)$
4B	$H_2O(g) \rightleftharpoons 2\underline{H} + \underline{O}$
5B	$\frac{1}{2}H_2(g) \rightleftharpoons \underline{H}$
6B	$CO + \frac{1}{2}O_2 \rightleftharpoons CO_2$
Gas Control Volume Reactions	
1G	$CO + \frac{1}{2}O_2 \rightleftharpoons CO_2$
2G	$H_2 + \frac{1}{2}O_2 \rightleftharpoons H_2O$

*The carbon boil reaction

B denotes BCV and G denotes GCV

populations of C, O, H, and Fe stays constant in both control volumes. The final two constraints come from the assumption that N_2 is inert, so any nitrogen that enters either control volume exits without reacting. The set of simultaneous equations that result from the equilibrium assumption are shown in Table III. This set of equations is solved numerically at each time step of the simulation to ensure that equilibrium exists at all times.

2.3 Material Balances

The final necessary element of an EAF model is a dynamic material balance. The material balance equations keep track of mass in-flow, mass out-flow, and the transport of compounds between the furnace control volumes. Material balances are written around both the bath control volume and the gas control volume. The gases in the BCV represent both the bubbles of CO created from the carbon boil reaction and a small amount of gas that does not mix completely with the free-board gas.

Each event that takes place in the furnace does so in a particular control volume. For instance, air infiltration contributes to the mass of the gas control volume and oxygen lancing contributes to the mass of the bath control volume. The segregation of the furnace into two control volumes is necessary in order for the model to be able to differentiate between oxygen that enters by infiltration and oxygen that is lanced directly into the bath. Without separate control volumes, both would contribute equally to the oxygen content of the bath which is not physically valid. The two control volume arrangement allows for a resistance to be placed between the free-board gas (GCV) and the bath (BCV) so that the model is able to limit the mixing of the two control volumes, similar to a real furnace system.

The two control volumes are able to exchange gaseous compounds using two different mechanisms. The first mechanism is convection from the BCV to the GCV and is justified by the large amounts of carbon monoxide generated by the carbon boil reaction. If the BCV reaction mechanisms generate more gas than a pre-specified limit, the excess gas is convected into the gas control volume. The BCV gas limit is set such that the bath volume is doubled by the gas present during the carbon boil[10].

The second mechanism for control volume gas exchange is a concentration difference driven flux. This type of transport allows the transfer of gas from a control volume of high concentration to a control volume of lower concentration, no matter the direction. The rate of transfer of gas across the interface is proportional to the contact area, the concentration difference, and a mass transfer coefficient. The mass transfer coefficient is a bulk transfer term and therefore not related to specific chemical properties. This mechanism of transport allows a small amount of oxygen from air infiltration to reach the bath. The equation describing this transport mechanism is:

$$R_i = A \cdot k \cdot (y_i^{BCV} - y_i^{GCV}) \quad (7)$$

R_i	molar rate of transfer of i to the GCV
A	contact area between control volumes
k	mass transfer coefficient
y_i^{BCV}	gas mole fraction in the bath control volume
y_i^{GCV}	gas mole fraction in the gas control volume

The actual material balance equations are based upon the classical conservation equation:

$$Rate\ of\ Accumulation = Rate\ In - Rate\ Out \quad (8)$$

Note that a term for generation by chemical reaction is not included in the material balance equation. This is because the generation term will be accounted for by the chemical equilibrium portion of the model. Before the material balance is called, the equilibrium state is calculated so equilibrium is forced to exist at all time steps of the simulation. A limit is also specified for the amount of gas present in the gas control volume. The volume, pressure, and temperature of the GCV stay rel-

Table III: Equilibrium Equations

No.	Equation	Description
	Bath Control Volume Equations	
1	$N^B_{CO} + N^B_{CO_2} + N^B_C - C^B_{tot} = 0$	Conservation of Carbon Atoms
2	$N^B_{CO} + 2N^B_{CO_2} + 2N^B_{O_2} + N^B_{FeO} + N^B_{H_2O} + N^B_{\underline{O}} - O^B_{tot} = 0$	Conservation of Oxygen Atoms
3	$2N^B_{H_2O} + 2N^B_{H_2} + N^B_{\underline{H}} - H^B_{tot} = 0$	Conservation of Hydrogen Atoms
4	$N^B_{Fe} + N^B_{FeO} - Fe^B_{tot} = 0$	Conservation of Iron Atoms
5	$\omega^{B\,2}_{FeO} - K^2_1 * P^B_{O_2} * \omega^{B\,2}_{Fe} = 0$	Equilibrium of Reaction 1B
6	$\omega^{B\,2}_{\underline{O}} - K^2_2 * P^B_{O_2} = 0$	Equilibrium of Reaction 2B
7	$P^B_{CO} - K_3 * \omega_C \omega_{\underline{O}} = 0$	Equilibrium of Reaction 3B
8	$\omega^B_{\underline{O}} \omega^B_{\underline{H}} - K_4 * P^B_{H_2O} = 0$	Equilibrium of Reaction 4B
9	$\omega^{B\,2}_{\underline{H}} - K^2_5 * P^B_{H_2} = 0$	Equilibrium of Reaction 5B
10	$P^{B\,2}_{CO_2} - K^2_6 * P^{B\,2}_{CO} * P^B_{O_2} = 0$	Equilibrium of Reaction 6B
	Gas Control Volume Equations	
1	$N^G_{CO} + N^G_{CO_2} - C^G_{tot} = 0$	Conservation of Carbon Atoms
2	$N^G_{CO} + 2N^G_{CO_2} + 2N^G_{O_2} + N^G_{H_2O} - O^G_{tot} = 0$	Conservation of Oxygen Atoms
3	$2N^G_{H_2O} + 2N^G_{H_2} - H^G_{tot} = 0$	Conservation of Hydrogen Atoms
4	$P^{G\,2}_{CO_2} - K^2_6 * P^{G\,2}_{CO} * P^G_{O_2} = 0$	Equilibrium of Reaction 1G
5	$P^{G\,2}_{H_2O} - K^2_7 * P^{G\,2}_{H_2} * P^G_{O_2} = 0$	Equilibrium of Reaction 2G

N^G_i is the total moles of i in the GCV
X^G_{tot} is total moles of X atoms in the GCV
ω^B_i is the weight percent concentration of i in the BCV
P^G_i is the partial pressure of i in the GCV
K_i is the equilibrium constant for chemical reaction i
Superscripts B or G denote a compound of the BCV or GCV, respectively

atively constant, so the amount of gas must also stay constant. The excess gas is convected out through the fourth hole to maintain the correct amount of gas in the free-board. The 17 material balances generate a set of ordinary differential equations and are shown in Table IV.

Where possible, the model has been developed to use physically-significant parameters instead of fitting parameters. In addition to furnace operating parameters like electrical and burner profiles, carbon addition schedules, and oxygen lancing schedules, the model requires geometry parameters like furnace diameter, and total opening area for infiltration.

3 MODEL BEHAVIOR

Figure 6 shows a set of operating profiles for a typical EAF operation. The figure gives the times for all furnace operations including oxygen lancing, burner operation, carbon addition, and carbon injection.

Figures 7 and 8 show the raw output from the model for a simulated furnace that is 22 feet in diameter and has a capacity of 170 tons. The operating profile that generates the data in these figures is the same as that discussed above. The figures contain plots of the molar amounts of all of the compounds present in the furnace with time for both of the control volumes.

The gas control volume plots in Figure 7 show the amounts of the six free-board gas components. All of the gases except oxygen show changes while charging takes place at 22 and 36 minutes. When oxygen lancing first starts, 7 minutes into the first melt-down, CO, CO_2, and H_2 levels rise dramatically while H_2O levels drop. These gas levels return to their initial states during the second and third charges. The second charge melt-down conditions are much like those of the first melt-down. The carbon monoxide and hydrogen plots show two large, flat peaks that correspond to the first two charge melt-downs. The first two peaks are followed by two shorter and sharper peaks that correspond to carbon running out in the BCV and the start of carbon injection, respectively. Carbon dioxide levels stay relatively constant until near the end of the heat. Water and nitrogen levels both drop during melting of the first two charges and rise toward the end of the heat. Oxygen is not predicted to be present in the free-board until late in the heat.

Figure 8 shows the molar amounts of ten of the eleven BCV compounds during the heat (N_2 has been omitted). Carbon monoxide is the only compound in the BCV that shows a correlation with the operating practice. The first two melt-downs and the carbon injection can be seen clearly in the CO plot. Seven other compounds' profiles show a relationship with the amount of carbon in the BCV. CO_2, H_2O, FeO, and $\underline{O}$ begin to change to non-zero values after the carbon is consumed in the BCV. In contrast, $\underline{H}$ levels are predicted to decline after the carbon is consumed.

Table IV: Furnace Model Material Balances

No.	Equation
	BCV Material Balances
1	$\frac{dN_C^B}{dt} = F_{inj} + \omega_C^{scrap} * F_{melt} * \frac{MW_C}{MW_{Fe}}$
2	$\frac{dN_{CO}^B}{dt} = -y_{CO}^B * F_{out}^B - R_{CO}$
3	$\frac{dN_{CO_2}^B}{dt} = -y_{CO_2}^B * F_{out}^B - R_{CO_2}$
4	$\frac{dN_{O_2}^B}{dt} = F_{lance} - y_{O_2}B * F_{out}^B - R_{O_2}$
5	$\frac{dN_O^B}{dt} = 0.0$
6	$\frac{dN_{Fe}^B}{dt} = F_{melt}$
7	$\frac{dN_{FeO}^B}{dt} = 0.0$
8	$\frac{dN_{H_2O}^B}{dt} = -y_{H_2O}^B * F_{out}^B - R_{H_2O}$
9	$\frac{dN_{H_2}^B}{dt} = -y_{H_2}^B * F_{out}^B - R_{H_2}$
10	$\frac{dN_H^B}{dt} = 0.0$
11	$\frac{dN_{N_2}^B}{dt} = -y_{N_2}^B * F_{out}^B - R_{N_2}$
	GCV Material Balances
12	$\frac{dN_{CO}^G}{dt} = y_{CO}^B * F_{out}^B - y_{CO}^G * F_{out}^G + R_{CO}$
13	$\frac{dN_{CO_2}^G}{dt} = y_{CO_2}^B * F_{out}^B - y_{CO_2}^G * F_{out}^G + F_{burner} + R_{CO_2}$
14	$\frac{dN_{O_2}^G}{dt} = y_{O_2}^B * F_{out}^B - y_{O_2}^G * F_{out}^G + y_{O_2}^{air} * F_{infil} + R_{O_2}$
15	$\frac{dN_{H_2O}^G}{dt} = y_{H_2O}^B * F_{out}^B - y_{H_2O}^G * F_{out}^G + 2F_{burner} + R_{H_2O}$
16	$\frac{dN_{H_2}^G}{dt} = y_{H_2}^B * F_{out}^B - y_{H_2}^G * F_{out}^G + R_{H_2}$
17	$\frac{dN_{N_2}^G}{dt} = y_{N_2}^B * F_{out}^B - y_{N_2}^G * F_{out}^G + R_{N_2}$

Superscript B and G denote in the BCV and the GCV

N_i = moles of i in the system

MW_C = mol. wt. of carbon

MW_{Fe} = mol. wt. of iron

R_i = concentration driven molar flow of i to the GCV (gmol/s)

F_{inj} = rate of carbon injection (gmol/s)

ω_C^{scrap} = wt. fraction carbon in scrap

F_{melt} = rate of melting (gmol/s)

y_i = mole fraction of i in the gas phase

F_{burner} = molar rate of methane flow to burner (gmol/s)

F_{out} = molar gas outflow rate (gmol/s)

y_i^{air} = mole fraction of i in air

F_{infil} = molar rate of air infiltration (gmol/s)

F_{lance} = molar rate of oxygen lancing (gmol/s)

F_{spray} = molar rate of water spray on electrode (gmol/s)

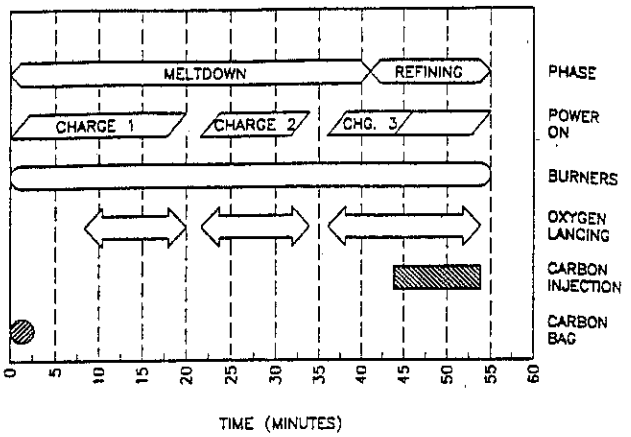

Operation	Amount
Power	40-80 MW
Burners (During Power On)	740 SCFM CH_4
Burners (During Power Off)	280 SCFM CH_4
Oxygen Lancing	2,150 SCFM
Carbon Injection	100 lb./min.
Carbon Bag	5,000 lb.

Figure 6: EAF Operating Parameters

Figure 9 shows the off-gas composition profile as calculated from the data in the GCV plot. Before oxygen lancing is started in the first melt-down, carbon dioxide is the main component of the off-gas at 19% (by volume). During lancing, CO_2 drops to be 16% of the off-gas while CO is the main component with a composition at 24%. Hydrogen also climbed from 2% to 3% during this same period. At 38 minutes, during the third charge melt-down, carbon monoxide and hydrogen concentrations drop to zero because all of the carbon in the BCV has been consumed. During the ten minutes of carbon injection that begin 43 minutes from the start, carbon dioxide is the major component of the off-gas at an average concentration of 22%.

Information about the volumetric flow of off-gas is useful in assessing the performance of the existing furnace gas cleaning system or designing a new one. Off-gas volume information may also help to locate periods when the furnace "puffs" due to high gas release rates. Figure 10 shows the predicted off-gas volume during the simulation. The figure shows that the gas generation rate is not constant, but varies from 14,000 to 15,700 SCFM. The off-gas flow rate is highest during the first two charge melt-downs when carbon is present and oxygen is being lanced into the furnace.

To evaluate the behavior of the furnace, three separate measures are used. The ratio of the total carbon monoxide to the total carbon dioxide released (CO/CO_2 ratio) is one method of judging the utilization of chemical

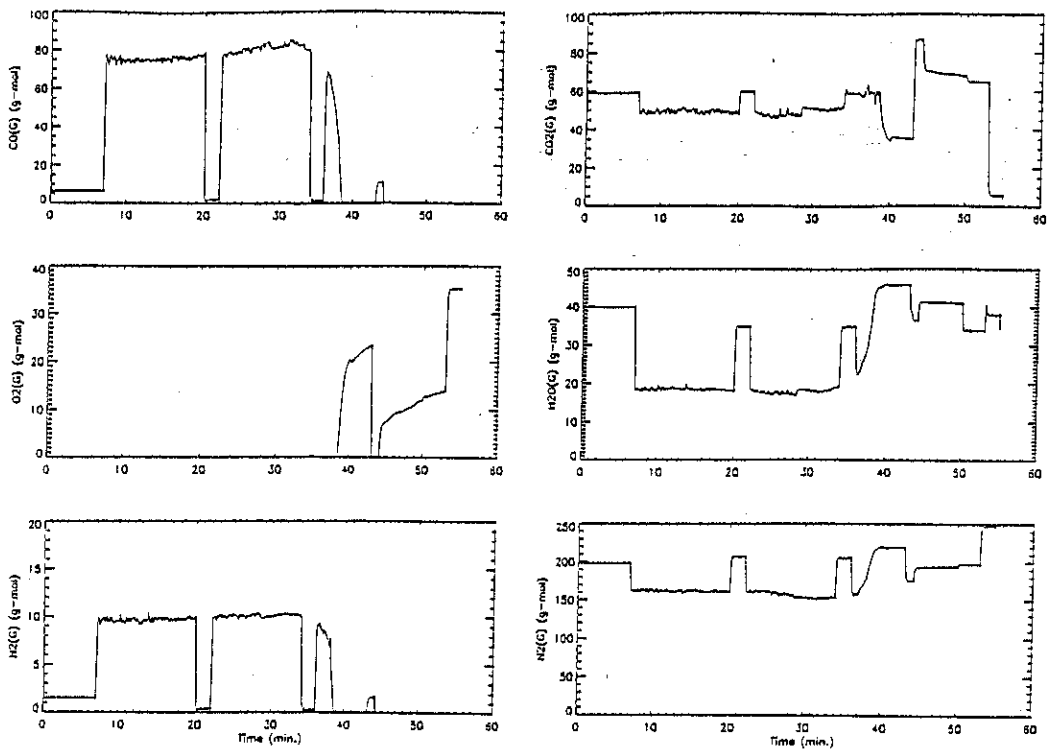

Figure 7: Gas Control Volume Furnace Compounds - Base Case

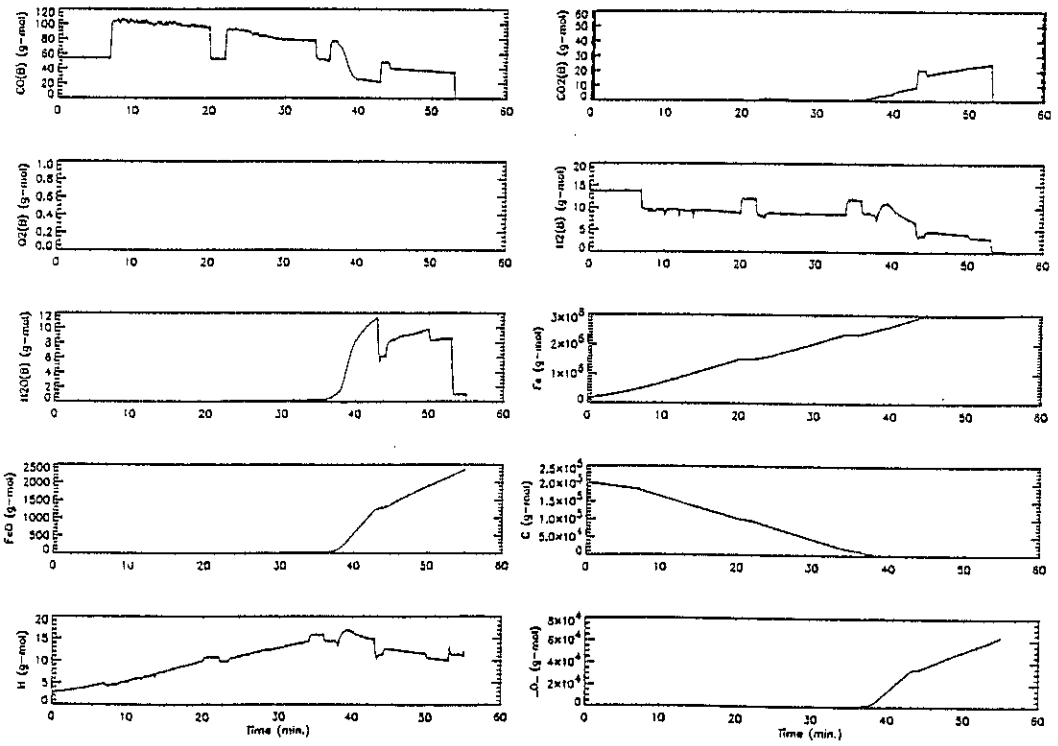

Figure 8: Bath Control Volume Furnace Compounds - Base Case

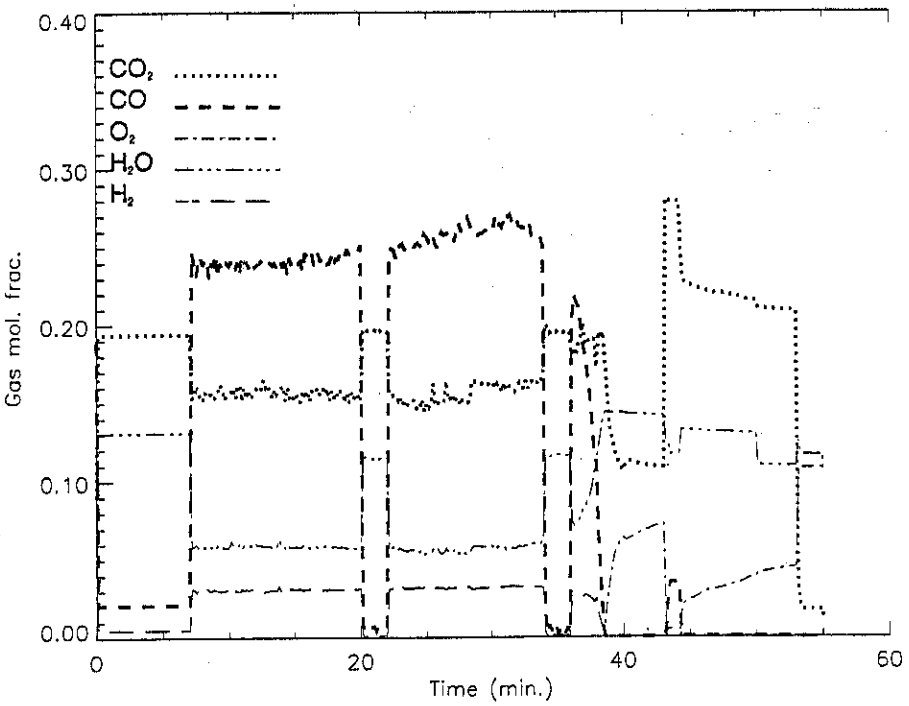

Figure 9: Off-Gas Volume for Base Case

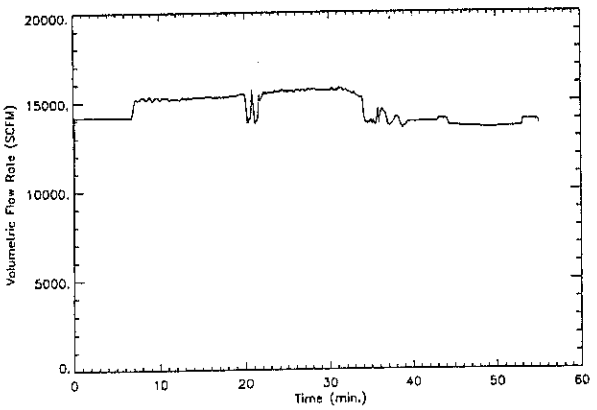

Figure 10: Furnace Off-Gas Volumetric Flow

energy in the furnace. If the CO/CO_2 ratio is high, then the furnace is producing a great deal of carbon monoxide and has room for improvement by combusting some CO. The utilization of iron to product is a second measure of furnace performance. A high utilization of iron is desirable in order to minimize the amount of iron in the slag. A third measure of furnace behavior is the peak off-gas volumetric flow.

Most furnace gas cleaning systems are sized according to the estimated peak off-gas flow, so if the peak flow is lowered, the system can be sized to be smaller. The peak flow is a function of both the fourth hole gas flow and the fourth hole H_2 and CO concentrations. The combustibles content of the gas is important because it determines the amount of infiltration air required at the combustion gap to burn the remaining H_2 and CO. It is therefore necessary to minimize both the fourth hole off-gas flow rate and the fourth hole combustibles content in order to minimize the peak off-gas flow rate.

The base case simulation is predicted to have a CO/CO_2 ratio of 0.756. The iron utilization is 99.92%, and the peak off-gas volumetric flow rate is 15,700 SCFM. These numbers will be used to compare cases posed in the following section.

4 MODEL CASE STUDY

Using the previously discussed furnace heat as a base case, a series of additional simulations have been run in order to find the effects of changing certain operating parameters on the behavior measurements. Two of the operating parameters that have been studied are the use of excess oxygen in the burners and the carbon addition rate.

A recent trend in EAF steel-making is the use of post-combustion to reduce the furnace energy requirements and reduce the amount of carbon monoxide present in the fourth hole gases. Several papers in the literature have shown the benefits of post-combustion[1,11,12,13,14].

4.1 Case 1

One form of post-combustion can be implemented relatively simply by introducing an excess amount of oxygen into the burner. The extra oxygen is free to enter the free-board and combust more carbon monoxide, providing extra energy to the furnace.

Figure 11 shows the off-gas composition profile for a simulation which introduces oxygen at 100% excess (stoichiometric) into the furnace through the burners. The CO/CO_2 ratio for this case is 0.651. This corresponds to a reduction of total CO release by 729 lb. compared to the base case. The combustion of 729 lb. of CO will yield 915 kW-hr of energy or ,in this case, 5 kW-hr/ton of steel. The iron utilization for this case is 99.89%. The iron utilization is lower than the base case because some of the extra oxygen put into the furnace reacts with the bath. The peak off-gas volumetric flow rate is 17,000 SCFM. The volumetric flow rates for this and the base case are not the same, however this case may have a lower peak off-gas flow since it releases less combustibles. Table V gives a comparison of each case examined.

An examination of the raw data for this case (not shown) reveals that carbon is completely consumed approximately 32 minutes into the heat, four minutes earlier than in the base case. The extra oxygen provided through the burners makes faster carbon consumption possible.

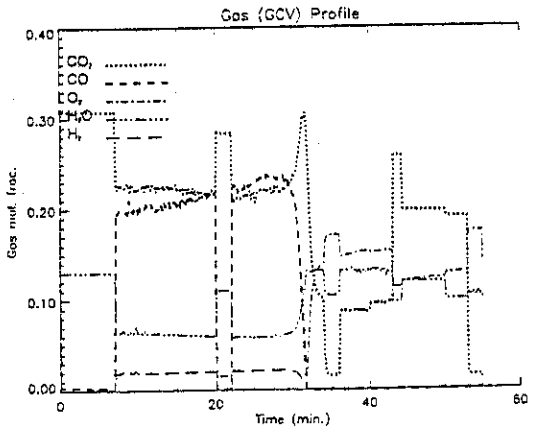

Figure 11: Off-Gas Composition for 100% Excess Burner O_2

4.2 Cases 2 and 3

The second simulated case injects 5,000 lb. of carbon continuously into the furnace instead of adding it all at the beginning of the heat. The base case simulation consumes the entire amount of carbon in 38 minutes, so the injection rate used is 132 lb./min. for 38 minutes. Figure 12 shows the off-gas composition profile for this case.

The profile appears to be similar to that of the base case, with only a slight difference in the carbon monoxide and carbon dioxide concentrations during the first and second charge melt-downs. The CO/CO_2 ratio for this change in operation is 0.715, which is slightly less than the base case's 0.756. The reduction in CO is estimated to be 276 lb. for the entire heat or 1.5 lb. CO/ton of steel. This translates to 347 kW-hr or 1.9 kW-hr/ton of savings if all of the energy remains in the furnace. The peak off-gas volumetric flow rate for this scenario is about 15,700 SCFM, the same as the base case.

Only a small improvement in performance is observed because the amounts of carbon and oxygen put into the furnace have not changed. The addition of excess oxygen through the burners will provide extra oxygen which will reduce the CO/CO_2 ratio more dramatically.

The third case injects carbon over 53 minutes at a lower rate of 94 lb./min. The gas composition profile is not shown, but the model predicts a CO/CO_2 ratio of 0.390 for this case. In the base case and case 2, oxygen is the limiting reactant for the carbon combustion reaction whereas in this case carbon is the limiting reactant. Once carbon is consumed, left-over oxygen is free to convert carbon monoxide to carbon dioxide. The peak off-gas flow rate for this case is 15,600 SCFM and the iron utilization is 99.97. Iron utilization is increased in this

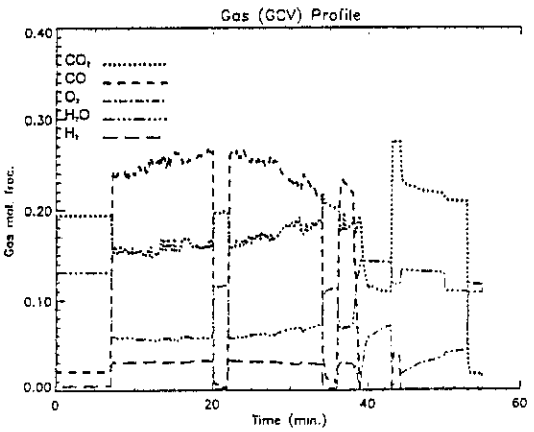

Figure 12: Off-Gas Composition for Continuous Carbon Injection

case because the period of carbon injection is so long that oxygen is not able to come into contact with the bath to react for very long.

Table V: Furnace Performance Comparison

Case	Description	Carbon Added (lb.)	CO/CO_2	Fe Util. (%)	Peak Off-Gas Flow (SCFM)
	Base Case	6,000	0.756	99.92	15,700
1	100% Excess O_2 in burners	6,000	0.651	99.89	17,000
2	Cont. Carbon Inj. (38 min.)	6,000	0.715	99.92	15,700
3	Cont. Carbon Inj. (53 min.)	6,000	0.390	99.97	15,600
4	100% Exc. O_2 and Cont. Inj. (38 min.)	6,000	0.458	99.90	17,000

4.3 Case 4

Case 4 simulates both continuous injection (38 minutes) and excess O_2. The gas profile for this case is shown in Figure 13. The gas composition looks similar to the base case profile during the first charge melt-down. During this period, carbon builds up in the BCV because there is not enough oxygen available to burn it all immediately. When oxygen lancing starts, 7 minutes into the heat, the carbon levels immediately begin to decline. CO drops off during the second melt-down when the BCV carbon is almost completely depleted. Once the carbon is gone, there is plenty of oxygen available to combust any carbon monoxide that is produced and carbon dioxide is the major component of the off-gas for the rest of the cycle.

The CO/CO_2 ratio for this case is predicted to be 0.458, a large improvement from the base case ratio of 0.756. The change in CO emissions from the base case is 1.2 tons, which translates to a potential energy savings of 16 kW-hr/ton. This case has a peak off-gas flow rate of 17,000 SCFM.

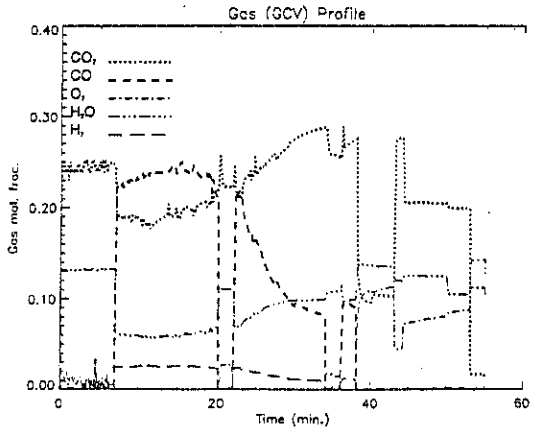

Figure 13: Gas Profile for Both Continuous Carbon Injection and 100% Excess O_2

5 CONCLUSIONS

A model of the electric arc furnace has been developed based upon a two control volume concept using equilibrium chemistry and dynamic material balances. Gas transport between the two control volumes is controlled by a convective boil-off rate and a concentration driven mass transport. This model is able to simulate the effects of oxygen lancing, carbon injection, burner operation, air infiltration, and electrical power input. It predicts both the off-gas conditions (volumetric flow and composition) and bath chemistry.

Important components inside of the furnace are included from all three phases: bath, slag, and gas. The selection of the compounds to include was performed by noting the important components as well as the components of highest population inside of the furnace.

The EAF model predicts a reduction of the total carbon monoxide released from the furnace when excess oxygen is introduced into the furnace through the burners.

A small reduction in the carbon monoxide release is predicted from continuously injecting carbon instead of adding large amount at once.

6 FUTURE WORK

The development of this EAF model is on-going and therefore we have several plans for improvement and modification. Experimental verification of the model is essential to the improvement of its accuracy. It is the authors' intention to obtain operating data from as many different furnaces as possible in order to ensure good generalization by the model to different furnace sizes and practices.

An energy balance around the furnace is also currently under formulation. With the energy balance in place, the model is expected to provide even more practical information on the operation of the furnace. The energy balance is planned to include heat transfer terms that correspond to losses to the water cooling system and the transfer of energy to unmelted scrap in addition to energy terms for the addition and removal of mass from the furnace. The fully implemented energy balance model will be able to predict bath temperatures as well as the energy demand and time needed to reach tapping conditions.

After the complete furnace model has been verified and calibrated, an investigation into the optimal oper-

ation of the furnace will be performed. The method of dynamic optimization will be used on the model to predict the best operating strategies to achieve specific performance objectives. Performance objectives can include one or several goals such as reducing tap-to-tap times, reducing total CO emissions, minimizing the total electrical input to the furnace, or a weighted sum of multiple objectives.

The end goal of this research is to have a general model that practitioners can use to predict bath and gas conditions as well as to find better operating strategies.

ACKNOWLEDGEMENT

We would like to acknowledge the financial support of Goodfellow Consultants Texas, Inc. for our first year of research in this area.

REFERENCES

1. Vonesh Jr., F. A. and Perrin, N. G. "Post-combustion for the electric arc furnace," Iron and Steel Engineer. Vol. 72, No. 6, pp. 30-32.
2. Billings, S.A., Boland, F.M., and Nicholson, H. "Electric Arc Furnace Modeling and Control," Automatica. Vol. 15, No. 2, pp. 137-48.
3. Boland, F.M. and Nicholson, H. "Estimation of the states during refining in electric-arc-furnace steelmaking," Proc. IEEE Control & Science. Vol. 124, No. 2, pp. 161-6.
4. Woodside, C.M., Pagurek, B., et. al. "Singular Arcs Occurring in Optimal Electric Steel Refining," IEEE Trans. Aut. Contr. Vol. AC-15, No. 5, pp. 549-56.
5. Thibault, Jules, "On Finite-Difference Solutions to the Heat Equation In Spherical Coordinates," Numerical Heat Transfer. Vol. 12, pp. 457-474.
6. Elliott, J. F. "The Chemistry of Electric Furnace Steelmaking," Electric Furnace Proceedings (1974).
7. Lankford, W.T., et. al. The Making, Shaping, and Treating of Steel, Herbick and Held, Pittsburgh, PA. 1985.
8. Sims, C.E., Electric Arc Furnace Steelmaking, Volume II, Interscience Publishers, New York, NY. 1963.
9. Elliott, J. F. The Physical Chemistry of Steelmaking. M.I.T. Press, Cambridge, Mass. 1956.
10. Bodsworth, C. Physical Chemistry of Iron and Steel Manufacture. Longmans, Green and Co. Ltd., London, Great Britain, 1963.
11. Grieshaber, C., Feldermann, C., and Jones, J. "Considerations for a Post-Combustion Strategy," 1995 Electric Furnace Conference Proceedings.
12. Perrin, N., Devaux, M., et. al. "Industrial Use of ALARC-PC Post-Combustion Technology Worldwide," Proc. 5th European Electric Steel Conference.
13. Slootman, F. and Buffenoir, M. "Effect of post-combustion on the heat and mass balances of an electric arc furnace," Proc. 5th European Electric Steel Congress.
14. McManus, G. J. "Electric Furnace post-combustion takes off," Iron and Steel Engineer. Vol. 72, No. 4, pp. 90-91.

For further information on this paper, please contact W. Fred Ramirez at Campus Box 424, Department of Chemical Engineering, University of Colorado, Boulder, Colorado 80309-0424, by phone at (303) 492-8660, or email at `Fred.Ramirez@Colorado.EDU`.